Peltonen, Joonas; Virtanen, Pauli; Meschke, Matthias; Koski, J.V.; Heikkilä, Tero; Pekola, Jukka

Thermal conductance by the inverse proximity effects in a superconductor

Published in:
Physical Review Letters

DOI:
10.1103/PhysRevLett.105.097004

Published: 27/08/2010

Document Version
Publisher's PDF, also known as Version of record

Please cite the original version:
Peltonen, J., Virtanen, P., Meschke, M., Koski, J. V., Heikkilä, T., & Pekola, J. (2010). Thermal conductance by the inverse proximity effects in a superconductor. *Physical Review Letters*, *105*(9), 1-4. Article 097004. https://doi.org/10.1103/PhysRevLett.105.097004

Thermal Conductance by the Inverse Proximity Effect in a Superconductor

J. T. Peltonen, P. Virtanen, M. Meschke, J. V. Koski, T. T. Heikkilä, and J. P. Pekola
Low Temperature Laboratory, Aalto University, P.O. Box 13500, FI-00076 AALTO, Finland
(Received 2 March 2010; published 27 August 2010)

We study heat transport in hybrid lateral normal-metal–superconductor–normal-metal structures. We find the thermal conductance of a short superconducting wire to be strongly enhanced beyond the BCS value due to the inverse proximity effect, resulting from contributions of elastic cotunneling and crossed Andreev reflection of quasiparticles. Our measurements agree with a model based on the quasiclassical theory of inhomogeneous superconductivity in the diffusive limit.

DOI: 10.1103/PhysRevLett.105.097004 PACS numbers: 74.45.+c, 07.20.Mc, 74.25.fc

In a bulk superconductor at the lowest temperatures, thermal conductivity is exponentially suppressed compared to the linear temperature dependence expected from the Wiedemann-Franz law [1]. The residual heat conduction at temperatures $k_B T \ll \Delta$ is only due to quasiparticles (QPs) at energies above the superconducting energy gap Δ, whereas Andreev reflection completely blocks the subgap flow of energy [2]. This explains why at such temperatures superconductors are poor conductors of heat, and their thermal conductivity can often be considered negligible. In hybrid mesoscopic structures with small normal-metal islands and short superconducting wires, the picture changes considerably, and heat flow through a superconductor can become essential [3]. When a superconductor (S) is brought into good contact with a normal metal (N) through a transparent metal-to-metal contact, properties of the N are modified by the widely studied proximity effect [4–7]. Close to the interface, also the S is modified by the *inverse* proximity effect: The energy gap is diminished and the subgap density of states is nonzero [8,9]. Andreev reflection takes place on the scale of the superconducting coherence length ξ_0, so that after a distance L into the superconductor a subgap QP survives with probability $\sim e^{-L/\xi_0}$. Thermal conductance from subgap energies is caused by those QPs which have not Andreev reflected back before reaching the other end of the superconductor. This corresponds to a combined effect of elastic cotunneling and crossed Andreev reflection [10], as both processes carry energy current in the same direction. As a result, the QP-mediated thermal relaxation through an S wire of length not much larger than ξ_0 is greatly enhanced. Contrary to dying out exponentially at the lowest temperatures, it can dominate over other mechanisms, e.g., electron-phonon (e-ph) relaxation in the N wire.

In this Letter, we report an experimental study of the thermal conductance G_{th} of diffusive S wires under the influence of the inverse proximity effect. This is in contrast to most thermal transport experiments on Andreev interferometers [11–13], where G_{th} depends mainly on the properties of the proximized normal metal, and the focus has been on long range phase coherent effects. Previously, G_{th} of diffusive normal-metal–superconductor–normal-metal (NSN) structures with short S sections of length $L_S \ll \xi_0$ was theoretically investigated in Ref. [14]. Here, $\xi_0 = \sqrt{\hbar D_S/\Delta_0}$ with D_S denoting the diffusion constant of the superconductor, and Δ_0 is the bulk energy gap at zero temperature. In this Letter, we focus on S wires with length $L_S \gtrsim \xi_0$ in the diffusive limit $l \ll \xi_0, L_S$, where l is the elastic mean free path. Electrical transport in similar NSN structures has recently attracted a lot of theoretical and experimental interest [10,15]. When it comes to thermal transport properties, apart from early experiments on large area NSN sandwiches at higher temperatures [16], quantitative measurements of G_{th} in a lateral NSN structure are, to our knowledge, missing.

To probe G_{th} experimentally, we have fabricated a series of structures similar to the one in Fig. 1(a), which displays a typical sample together with the measurement scheme. The structures consist of two normal metal copper (Cu) islands of length $L_N \simeq 2.5$–$4\ \mu$m, width $W_N \simeq 200$–250 nm, and thickness $d_N \simeq 25$–30 nm, connected by a short superconducting aluminum (Al) wire of width $W_S \simeq 300$–400 nm and thickness $d_S \simeq 40$–50 nm, with the length L_S varying from sample to sample. Ends of the S wire are overlapping the N regions over a distance $L_O \simeq 200$–300 nm, as illustrated schematically in the inset in Fig. 1(a). When the N islands are held at different temperatures T_1 and T_2, heat current P_S flows through the superconductor, and for small temperature differences $\Delta T \equiv T_2 - T_1 \ll T \equiv (T_1 + T_2)/2$, one has $G_{\mathrm{th}}(T) = P_S/\Delta T$. Besides the direct NS contact to the short Al wire, each N island is connected via aluminum oxide tunnel barriers to four superconducting Al leads. These normal-metal–insulator–superconductor (NIS) tunnel junctions with an area of $(150$–$200) \times 200$ nm^2 and typical normal state resistance $R_T \simeq 20$–$100\ \mathrm{k}\Omega$ allow for the measurement of the electronic temperatures T_1 (island 1) and T_2 (island 2) and creation of the gradient ΔT, as discussed below in more detail.

To calculate G_{th} within the framework of nonequilibrium superconductivity, pair correlations in the S wire are

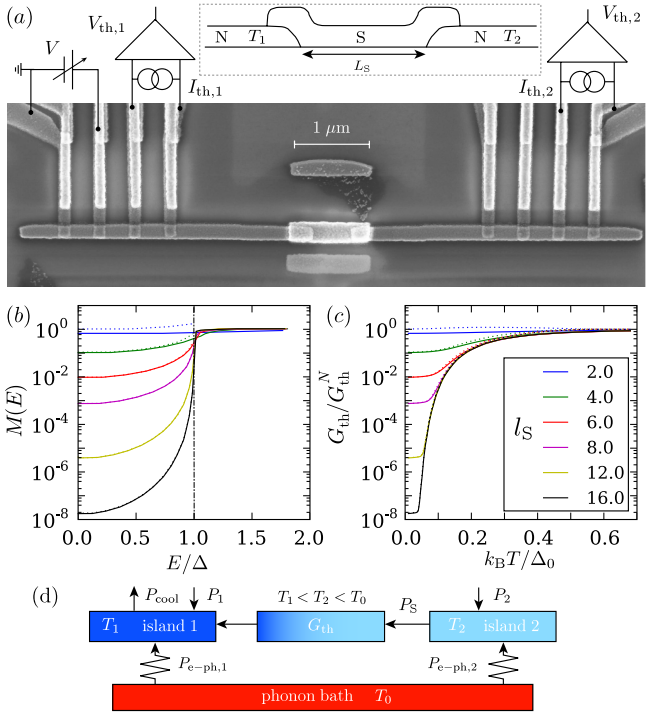

FIG. 1 (color online). (a) Scanning electron micrograph of a typical sample, together with the configuration for thermal conductance measurements. Two Cu islands are connected via a short superconducting Al wire with transparent NS interfaces. Four S electrodes (top of the image) are connected to each of the two N islands through tunnel barriers for electronic thermometry and temperature control. Inset: Sketch of the side profile of the NSN structure, consisting of an S wire connected via overlap junctions to two N reservoirs. (b) Heat transparencies and (c) thermal conductances from a numerical calculation (solid line) and an analytical approximation (dotted line) for an NSN structure with an S wire of the indicated length $l_S = L_S/\xi_0$. (d) Thermal model for the experimental setup as detailed in the text. Arrows indicate direction of heat flows at temperatures $T_1 < T_2 < T_0$.

described in terms of a position- and energy-dependent complex function $\theta(x, E)$. From a solution of the Usadel equations [4,17,18], it follows that G_{th} of a diffusive S wire of length $l_S = L_S/\xi_0$ between two N reservoirs is given by

$$G_{th} = \frac{G_N}{2k_BT^2e^2}\int_0^\infty dE E^2 M(E)\mathrm{sech}^2\left(\frac{E}{2k_BT}\right). \quad (1)$$

Here, $G_N = R_N^{-1}$ denotes the normal state electrical conductance of the S wire, and $M(E)$ is an energy-dependent heat transparency defined by $M(E)^{-1} = l_S^{-1}\int_0^{l_S} dx \cos^{-2}[\mathrm{Im}\theta(x, E)]$. The quantity $M(E)$ can be interpreted as the fraction of QPs which are able to diffuse through the S wire from one N reservoir to the other, relative to that in the normal state. In the BCS limit with $l_S \gg 1$, $M(E) = 1$ at $E > \Delta$, and it vanishes below the gap. In that case, defining $y = \Delta/k_BT$, we recover for $y \gtrsim 2$ from Eq. (1) the result

$$G_{th}^{BCS} \simeq 2G_NT(k_B/e)^2(y^2 + 2y + 2)e^{-y}. \quad (2)$$

On the other hand, in the normal state with $M(E) \equiv 1$, Eq. (1) reduces to the Wiedemann-Franz value $G_{th}^N = \mathcal{L}_0 G_N T$ with the Lorenz number $\mathcal{L}_0 = (\pi^2/3)k_B^2/e^2$.

Neglecting self-consistency of the order parameter and the overlaps of N and S, we can find an analytical approximation for G_{th} which includes subgap heat transport and describes how $M(E)$ starts to deviate from a step function as l_S decreases [18]. At energies $E < \Delta$ we have

$$M(E) \simeq 32\{\mathrm{Im}\tanh[(\theta_S - \theta_0)/4]\}^2 be^{-b}\coth(b/2), \quad (3)$$

with $b = l_S(2\sqrt{\Delta^2 - E^2}/\Delta_0)^{1/2}$, whereas $M(E) \simeq 1$ for $E > \Delta$. Here, $\theta_S = \mathrm{artanh}(\Delta/E)$ and θ_0 are the values of θ far in the superconductor and close to the NS interface, respectively. The value of θ_0 is found by considering the boundary condition for θ at the interface. In the limit of vanishing interface resistance it is determined mainly by the quantity $r = A_S\sigma_S^N/A_N\sigma_N^N$, which includes the cross sections and normal state conductivities of the S and N parts. In the zero temperature limit the normalized thermal conductance G_{th}/G_{th}^N saturates to the constant value $M(0)$ and grows as $\sim T^2$ at low temperatures. For $A_S/A_N \ll 1$ and $l_S \gtrsim 4$, we find $M(0) \simeq 32(3\sqrt{2} - 4)l_S\exp(-\sqrt{2}l_S)$. The result of Eq. (3) with $A_S/A_N \ll 1$ is compared to non-self-consistent numerical estimates in Fig. 1(b), and we see it to be valid for $l_S \gtrsim 4$. The G_{th} in Fig. 1(c) is consequently obtained by using this $M(E)$ in Eq. (1) and assuming a BCS temperature dependence for Δ. This is shown below to be in fair agreement with experiments, but especially at higher temperatures and for shorter samples self-consistent numerical calculations become necessary.

The samples were fabricated on an oxidized silicon substrate by electron beam lithography and three-angle shadow evaporation of the metals through a suspended resist mask. Based on resistivity measurements, we estimate $D_S \simeq 50$–75 cm^2/s and $l \simeq 10$ nm for aluminum. Together with the energy gap $\Delta_0 \simeq 200$ μeV for Al, we have $\xi_0 \simeq 100$–150 nm. The structures were measured through filtered signal lines in a ^{3}He-^{4}He dilution refrigerator with a base temperature below 50 mK. Here, we present measurements on four samples with the nonoverlapped S length L_S varying in the range 400 nm–4 μm. We refer to Table I for sample parameters and dimensions. We estimate the interface resistance of the direct transparent NS contacts to be less than 1 Ω. The strong electron-electron interaction in copper allows us to assume a well-defined local electronic temperature to exist on each island. Because of the relatively small size of the islands, we are able to probe and control these temperatures in the following way: As shown in Fig. 1(a), on each island i one pair of NIS junctions is biased by a battery-powered floating source at a fixed current $I_{th,i} \lesssim 0.005\Delta_0/eR_T$, $i = 1, 2$. Since QP tunneling in a NIS junction and therefore the current-voltage characteristic is strongly dependent on the normal metal temperature [19], the voltages $V_{th,i}$ act as

thermometers once calibrated against the cryostat temperature T_0 [20]. To create a temperature difference between the islands, the remaining pair of NIS junctions on island 1 is biased by a dc voltage $e|V| \lesssim 2\Delta$, making this SINIS structure function as an electronic refrigerator [21,22] due to energy-selective QP tunneling. On the other hand, the low bias current of the thermometer does not significantly affect the thermal balance of the island.

Figure 2 displays the measured electronic temperatures T_i for each sample at three representative bath temperatures T_0. For all T_0 displayed in Fig. 2, a drop in the temperature T_1 of island 1 is evident close to $e|V| \simeq 2\Delta$, where the cooling power of the SINIS refrigerator reaches its maximum. At the highest bath temperatures displayed, the temperature T_2 of the remote island first closely follows T_1, but at lower T_0 a strongly L_S-dependent difference develops. At the observed electronic temperatures, thermal conduction through the substrate is weak, and a difference between T_1 and T_2 as a function of V therefore reflects the thermal conductance G_{th} of the S wire. To characterize this thermal link between the islands, we choose to study the temperature drops $\Delta T_i \equiv T_i(V) - T_i(V = 0)$ at the optimal cooler bias voltage as a function of T_0. For consistency we performed several measurements on each sample, permuting the pairs of NIS junctions used for thermometry and refrigeration. The ratio $\Delta T_2/\Delta T_1$ has the advantage of being largely insensitive to the cooling power of the refrigerator junctions; i.e., it is unaffected by their R_T or other characteristics.

To analyze the dependence of the relative temperature drop $\Delta T_2/\Delta T_1$ on T_0, we utilize the thermal model of Fig. 1(d). Since the bias voltage V of the SINIS refrigerator is swept at a very low rate compared to the e-ph relaxation time, the system reaches a thermal steady state at each V, corresponding to the heat balance equations $P_{cool} - P_S - P_{e\text{-ph},1} - P_1 = 0$ and $P_S - P_{e\text{-ph},2} - P_2 = 0$ for island 1 and 2, respectively. We assume the islands to exchange energy via QP heat conduction along the S wire, described by G_{th} and the heat flow P_S. In addition, heat is removed from the cooled island, described by the power P_{cool} [22]. At the optimal cooler bias voltage, typical values of P_{cool} for the measured samples lie in the range 10–100 fW. Electrons on each island are thermally coupled to the island phonons at T_0 via e-ph coupling, modeled by the power flows $P_{e\text{-ph},i} = \Sigma \mathcal{V}_i(T_0^5 - T_i^5)$ [23]. Here, $\Sigma \simeq 2 \times 10^9$ W K^{-5}m^{-3} [19] is the e-ph coupling constant of Cu, and $\mathcal{V}_i$ is the volume of island i. Finally, the constant terms $P_i \simeq 1$ fW account for unavoidable parasitic heating from the electrical environment. We assume a low Kapitza resistance between the Cu island and substrate phonons, thereby neglecting any lattice cooling or heating. This allows us to fix the phonon temperature to T_0, i.e., the cryostat bath temperature. We neglect also the photonic heat conduction, because of mismatched impedances, as well as e-ph coupling within the superconductor due to the short length of the S wires [24].

Figure 3(a) displays the measured T_0 dependence of $\Delta T_2/\Delta T_1$ for the four samples. Predictions of the thermal model with G_{th} calculated by using Eqs. (1) and (3) with

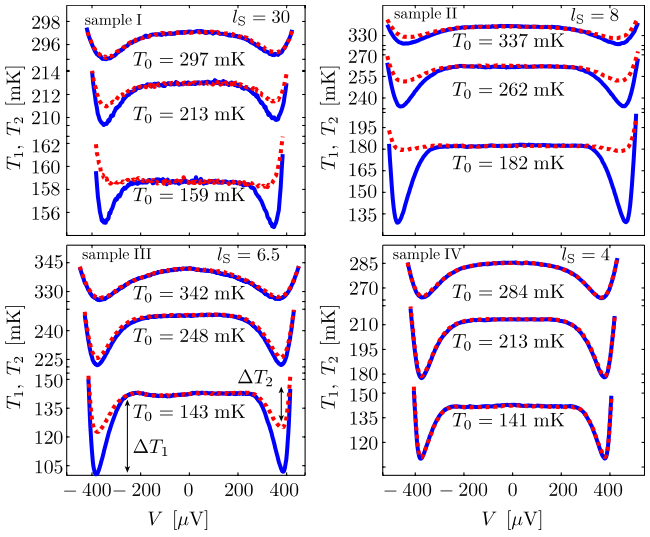

FIG. 2 (color online). Measured electronic temperatures T_1 (blue solid lines) and T_2 (red dotted lines) as a function of the voltage V across the SINIS refrigerator on island 1. Each panel shows data acquired at three different bath temperatures T_0. Sample I was refrigerated with only a single NIS junction; hence the voltage axis was scaled up by a factor of 2.

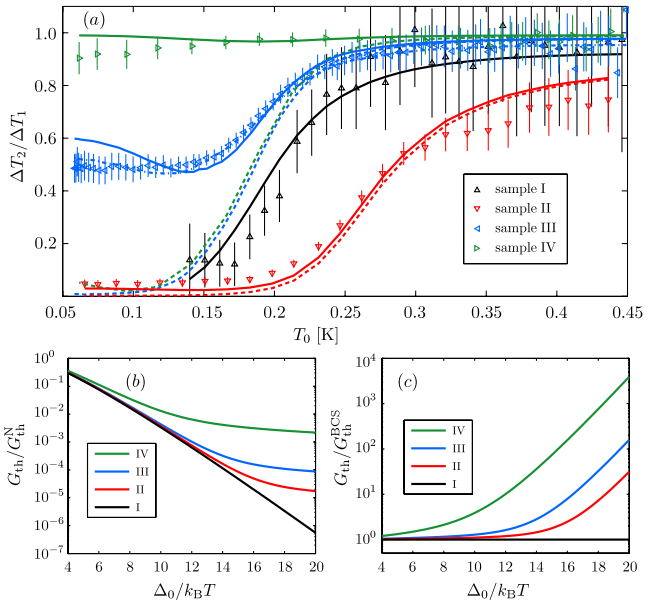

FIG. 3 (color online). (a) Temperature dependence of the relative temperature drop $\Delta T_2/\Delta T_1$. The symbols show the measured data, whereas the solid, dashed, and dash-dotted lines correspond to the thermal model with G_{th} based on Eq. (3), the $l_S \gg 1$ limit of Eq. (2), and a numerical solution of the Usadel equation, respectively. The error bars are based on the uncertainty in the temperature calibration of the NIS thermometers. (b),(c) T dependence of the G_{th} employed to produce the solid lines in (a), normalized to G_{th}^N in (b) and to G_{th}^{BCS} in (c).

TABLE I. Sample parameters; see the text for details.

Sample		I	II[a]	III	IV
Δ_0	[μeV]	190	230	185	185
L_S	[μm]	4.2	1.1	0.875	0.425
R_N	[Ω]	15	20	5	2
l_S		30	8	6.5	4

[a]Metals deposited in a different evaporator for this structure.

$r \simeq 2$ are shown in Fig. 3(a) as the solid lines. The dashed lines show the $l_S \gg 1$ limit described by Eq. (2). The lines in Figs. 3(b) and 3(c) further show G_{th} relative to its normal state and the BCS limit value, respectively. In all cases, the measured temperatures T_1 were used as input for solving the heat balance equation of island 2 to obtain T_2, and l_S and R_N were treated as fitting parameters with the values indicated in Table I. Similar results are obtained when the cooling power P_{cool} is calculated theoretically, and both heat balance equations are solved. In Fig. 3(a), the agreement between the model with the analytically approximated G_{th} (solid lines) and the measurements is reasonable for all the samples. For sample I with largest l_S, $\Delta T_2/\Delta T_1$ follows closely the BCS result, similar to sample II with a relatively large R_N. Most remarkably, for samples III and IV with the smaller l_S, the low temperature behavior of $\Delta T_2/\Delta T_1$ is strongly affected by the inverse proximity. The high values of $\Delta T_2/\Delta T_1$ at the lowest T_0 differ drastically from the prediction based on the BCS heat conductance alone (dashed lines). The dash-dotted blue line for sample III is based on G_{th} obtained from a self-consistent fully numerical solution of the Usadel equation in a 1D proximity circuit, including the overlap regions and the series N wires [18]. Compared to the analytical prediction, the lesser increase in $\Delta T_2/\Delta T_1$ at low temperatures can be partly attributed to an effective increase of l_S due to the proximity effect in the N parts. Linearizing the heat balance equation of island 2 for small ΔT gives $\Delta T_2/\Delta T_1 \simeq G_{th}/(G_{th} + G_{e\text{-ph},2})$, with $G_{e\text{-ph},2} \simeq 5\Sigma\mathcal{V}_2 T_0^4$ denoting the e-ph thermal conductance. Comparing the subgap and above-gap contributions of G_{th} to each other and to $G_{e\text{-ph},2}$, one can estimate the significance of the inverse proximity effect at low temperatures. For the long samples I and II with negligible subgap heat transport, $\Delta T_2/\Delta T_1$ drops below 0.5 approximately at the bath temperature at which $G_{e\text{-ph},2}$ becomes larger than G_{th}. On the other hand, for samples III and IV, the subgap conductance alone is larger than $G_{e\text{-ph},2}$ at all T_0 shown in Fig. 3(a), and $\Delta T_2/\Delta T_1$ remains above 0.5.

In summary, we have investigated the thermal conductance of short superconducting wires in the presence of the inverse proximity effect. We find the conductance to be strongly enhanced relative to that expected for a bulk superconductor, complementing earlier work on the thermal conductance of mesoscopic normal-metal wires in close proximity to superconductors. Our study helps understanding heat transport in mesoscopic structures, allowing one to either utilize or avoid the heat flows through proximized superconductors, e.g., in detector applications of hybrid normal-metal–superconductor structures or in electronic refrigeration.

We acknowledge financial support from the EU NanoSciERA project "NanoFridge" and the FP7 program "MICROKELVIN." We thank H. Courtois, F. Giazotto, and N. B. Kopnin for useful discussions. J. T. P. acknowledges financial support from the Finnish Academy of Science and Letters, and T. T. H. from the Academy of Finland and the ERC (Grant No. 240362-Heattronics).

[1] J. Bardeen, G. Rickayzen, and L. Tewordt, Phys. Rev. **113**, 982 (1959).
[2] A. F. Andreev, Sov. Phys. JETP **19**, 1228 (1964).
[3] H. Courtois *et al.*, Phys. Rev. Lett. **101**, 067002 (2008).
[4] W. Belzig *et al.*, Superlattices Microstruct. **25**, 1251 (1999).
[5] S. Guéron *et al.*, Phys. Rev. Lett. **77**, 3025 (1996).
[6] P. Dubos *et al.*, Phys. Rev. B **63**, 064502 (2001).
[7] H. le Sueur *et al.*, Phys. Rev. Lett. **100**, 197002 (2008).
[8] A. I. Buzdin, Rev. Mod. Phys. **77**, 935 (2005).
[9] M. A. Sillanpää *et al.*, Europhys. Lett. **56**, 590 (2001).
[10] A. Brinkman and A. A. Golubov, Phys. Rev. B **74**, 214512 (2006).
[11] For a recent review of the thermal transport experiments, see V. Chandrasekhar, Supercond. Sci. Technol. **22**, 083001 (2009).
[12] J. Eom, C. J. Chien, and V. Chandrasekhar, Phys. Rev. Lett. **81**, 437 (1998).
[13] Z. Jiang and V. Chandrasekhar, Phys. Rev. Lett. **94**, 147002 (2005); Phys. Rev. B **72**, 020502(R) (2005).
[14] E. V. Bezuglyi and V. Vinokur, Phys. Rev. Lett. **91**, 137002 (2003).
[15] See, e.g., S. Russo *et al.*, Phys. Rev. Lett. **95**, 027002 (2005); D. S. Golubev, M. S. Kalenkov, and A. D. Zaikin, *ibid.* **103**, 067006 (2009).
[16] G. Deutscher, P. Lindenfled, and R. D. McConnell, Phys. Rev. Lett. **21**, 79 (1968).
[17] K. D. Usadel, Phys. Rev. Lett. **25**, 507 (1970).
[18] See supplementary material at http://link.aps.org/supplemental/10.1103/PhysRevLett.105.097004 for a detailed description of our theoretical model.
[19] F. Giazotto *et al.*, Rev. Mod. Phys. **78**, 217 (2006).
[20] M. Nahum and J. M. Martinis, Appl. Phys. Lett. **63**, 3075 (1993).
[21] M. Nahum, T. M. Eiles, and J. M. Martinis, Appl. Phys. Lett. **65**, 3123 (1994).
[22] M. M. Leivo, J. P. Pekola, and D. V. Averin, Appl. Phys. Lett. **68**, 1996 (1996).
[23] M. L. Roukes *et al.*, Phys. Rev. Lett. **55**, 422 (1985).
[24] A. V. Timofeev *et al.*, Phys. Rev. Lett. **102**, 200801 (2009); **102**, 017003 (2009).